Low-temperature synthesis of crystalline GeSn with high Sn concentration by electron excitation effect

Low-temperature synthesis of crystalline GeSn with high Sn concentration by electron excitation effect

Toshiki Kimura,[1] Manabu Ishimaru,[1,*] Masayuki Okugawa,[2] Ryusuke Nakamura,[2] and Hidehiro Yasuda[3]

[1]*Department of Materials Science and Engineering, Kyushu Institute of Technology, Kitakyushu, Fukuoka 804-8550, Japan*

[2]*Department of Materials Science, Osaka Prefecture University, Sakai, Osaka 599-8531, Japan*

[3]*Research Center for Ultra-High Voltage Electron Microscopy, Osaka University, Ibaraki, Osaka 567-0047, Japan*

Abstract

The low-temperature synthesis of high-Sn-concentration GeSn is challenging in realizing flexible thin-film transistors and solar cells. Because of athermal processes, irradiation with energetic particles is anticipated to significantly reduce the processing temperature for device fabrication. Here, we demonstrated that polycrystalline Ge with ~30 at.% Sn can be realized at room temperature by the electron-beam-induced recrystallization of amorphous GeSn. We found that inelastic electronic stopping, the so-called electron excitation effect, plays an important role in the recrystallization of amorphous GeSn.

*E-mail: ishimaru@post.matsc.kyutech.ac.jp

Polycrystalline germanium-tin (GeSn) thin films on a flexible plastic substrate are anticipated as high-speed thin-film transistors and high-efficiency thin-film solar cells [1]. To realize this application, two breakthroughs are required: the increase in Sn concentration in the Ge matrix and the reduction in processing temperature. The solubility limit of Sn in Ge is ~1.1 at.% at 400 ºC [2]; therefore, the substitutional incorporation of Sn atoms into a diamond structure is difficult and Sn segregation easily occurs during the formation of GeSn. Several researchers have demonstrated that solid phase recrystallization from an amorphous phase can produce crystalline Ge including a large amount of Sn beyond the solubility limit [3-8]. Moreover, it is known that Sn addition causes the lowest crystallization temperature among various metal-induced crystallization techniques for amorphous Ge [1,9] because of the low eutectic temperature of the Ge-Sn binary system (~231 ºC). Indeed, Toko *et al*. [5] succeeded in fabricating GeSn with a composition of ~25 at.% Sn by annealing a crystalline Sn/amorphous Ge bilayer on SiO_2 at 70 ºC for 150 h.

In the previous studies of GeSn fabrication [3-8,10,11], amorphous phases have been crystallized by conventional heat treatment or laser annealing. Irradiation with energetic particles induces atomic rearrangements athermally; therefore, it is expected that the processing temperature for device fabrication will be significantly reduced [12]. For example, the recrystallization of amorphous alumina (Al_2O_3) was observed at room temperature under electron-beam irradiation [13], although its amorphous structure was maintained up to 700 ºC in the case of thermal annealing [14,15]. In addition, the material synthesis using irradiation fields can realize an atomic arrangement far from the equilibrium state, which is difficult to be obtained by conventional material synthesis techniques [16-18].

We have recently found that electron-beam-induced recrystallization occurs in amorphous Ge at room temperature [19,20], much lower than its crystallization temperature

(400-650 ºC) [21]. In the present study, we prepared amorphous GeSn by sputtering and examined its structural changes under electron-beam irradiation by *in situ* transmission electron microscopy (TEM). As a result, GeSn with ~30 at.% Sn was successfully fabricated at room temperature.

Amorphous GeSn thin films with a thickness of 40 nm were prepared by radio-frequency sputtering at a base pressure of $3x10^{-5}$ Pa. Square Sn chips of 5 x 5 mm^2 were placed on a Ge target with a diameter of 101.6 mm in order to control the Sn concentration. The GeSn thin films were deposited on a cleaved rock salt substrate at ambient temperature. The film and substrate were placed in distilled water, and then the floating film was recovered on a molybdenum grid [22]. The electron-beam-induced recrystallization behavior of as-sputtered samples was observed *in situ* by Hitachi H-7000 TEM. The beam current was monitored using a Faraday cage. The Sn concentration was measured using JEOL JEM-3000F equipped with an energy-dispersive x-ray (EDX) spectroscope.

Figure 1(a) shows a high-resolution TEM image along with a selected-area electron diffraction (SAED) pattern of an as-sputtered GeSn thin film obtained by placing 30 Sn chips on a Ge target. The high-resolution image shows a typical maze pattern and halo rings appear in the diffraction pattern: the as-sputtered specimen is amorphous and no marked phase separation occurs. Figure 1(b) shows the EDX spectrum of this specimen. In addition to the characteristic x-rays of Ge, the signals associated with Sn exist in the spectrum. The Sn concentration was estimated by the quantitative analysis of the EDX spectrum. The Sn concentration increases from 8.2 to 40.2 at.% with the number of Sn chips [Fig. 1(c)], and it is much higher than the solubility limit of Sn in crystalline Ge (~1.1 at.% at 400 ºC).

It was found that the amorphous GeSn thin films are crystallized by electron-beam irradiation. Figure 2(a) shows the electron-beam-induced structures of the specimen whose Sn

concentration is 22.8 at.% in the as-sputtered amorphous state. The SAED pattern in Fig. 2(a) was obtained from the thin film irradiated with a 75 keV electron beam at a flux of 8.7×10^{21} e/(m^2/s). Debye-Scherrer rings appear after crystallization, and they are indexed from the inside as 111, 220, and 311 of a diamond structure. No extra reflections due to the secondary phase are observed in the SAED pattern, suggesting the formation of homogeneous GeSn crystals. The bright-field TEM image of Fig. 2(b) reveals the formation of crystallites with a diameter of <10 nm. On the other hand, it was confirmed that a higher flux [7.9×10^{22} e/(m^2s)] induces coarse grains with a diameter of >100 nm [Fig. 2(d)]. In addition to the Bragg reflections resulting from the diamond structure, extra reflections corresponding to β-Sn, some of them are indicated by arrows, are observed in the vicinity of the 111 ring in Fig. 2(c).

It was found that the amorphous GeSn thin films were immediately crystallized when the electron flux was above the critical value. Figure 3 shows the flux dependence of crystallization as a function of Sn concentration. The flux was gradually increased for this experiment and the critical value for the amorphous-to-crystalline phase transformation was determined by observing the change in diffraction pattern from halo rings to Debye-Scherrer ones. It is apparent that the flux required for crystallization decreases with increasing Sn concentration. This means that crystallization occurs more easily in the amorphous GeSn with a higher Sn concentration. Crystallization under radiation environments is roughly caused by two effects: knock-on and electron excitation (ionization) effects. The latter becomes more pronounced with decreasing acceleration voltage, because slower electrons interact with the matter for a longer time. In Fig. 3, a 75 keV electron beam can induce crystallization at a lower flux than a 125 keV one. This suggests that the crystallization observed here is induced by the electron excitation effect rather than by the knock-on one. For further confirmation, we calculate the knock-on energy under the present irradiation condition. The maximum recoil

energy T_m is given by

$$T_m=2E(E+2m_0c^2)/Mc^2,$$

where E is the energy of the incident electron, m_0 the rest mass of the electron, c the velocity of light, and M the mass of the displaced atom. A 75 keV (125 keV) electron transfers energy up to 2.4 eV (4.2 eV) for a Ge atom and 1.5 eV (2.6 eV) for a Sn atom. These values are much smaller than the displacement energy required for the crystallization of amorphous Ge, *i.e.*, 7.2 eV (corresponding to E = 200 keV) [23]; therefore, we can conclude that inelastic electronic stopping stimulates the crystallization of amorphous GeSn. The recrystallization via the electron excitation effect was also observed in pure amorphous Ge [19,20,23].

Figure 4 shows the SAED patterns of GeSn thin films crystallized by electron-beam irradiation: (a) 8.2, (b) 20.0, (c) 22.8, and (d) 40.2 at.% Sn in the as-sputtered amorphous state. In all the diffraction patterns, the Debye-Scherrer rings resulting from the diamond structure appear. A weak halo ring due to Sn segregation is observed just outside the 111 ring in Figs. 4(c) and 4(d), suggesting the formation of amorphous and/or nanocrystalline Sn. The halo ring is not visible in Fig. 2(a), although the number of Sn chips is the same as that in Fig. 4(c): the critical concentration at which Sn segregation occurs is considered to be ~23 at.% Sn in the as-sputtered amorphous GeSn.

Note that the diameter of the Debye-Scherrer rings decreases with increasing Sn concentration, indicating the increase in lattice parameter. This suggests that Sn atoms are incorporated substitutionally into the Ge lattice. From the lattice parameter, the Sn concentration was roughly estimated on the basis of Vegard's law. The camera length was calibrated by the diffraction pattern of polycrystalline thallium(I) chloride. Figure 4(e) shows the Sn concentration of recrystallized GeSn as a function of the number of Sn chips. The lattice parameters of Ge and α-Sn were assumed to be 0.5658 and 0.6493 nm, respectively.

For comparison, the Sn concentration of as-sputtered amorphous GeSn, *i.e.*, Fig. 1(c), is also plotted. Even in the specimens without Sn segregation, there is a deviation of ~5 at.% between the Sn concentration estimated by EDX spectroscopy (for amorphous GeSn) and the lattice parameter (for crystallized GeSn). This is presumably due to the inaccuracy of Vegard's law that underestimates the Sn concentration. The difference in Sn concentration between the amorphous and crystalline GeSn becomes remarkable when the number of Sn chip sheets exceeds 50. This is attributed to the segregation of Sn, as confirmed by the results of electron diffraction experiments in Figs. 4(c) and 4(d). Note that the lattice parameter continuously increases even after the halo ring appears in the diffraction pattern: Sn atoms are continuously incorporated into the diamond structure.

Finally, we discuss how much temperature rise would occur during irradiation. The highest temperature rise T due to beam heating for a uniform film sample can be estimated using the following equations [24-26]:

$$T = W_0[1 + 2\ln(R / r_0)] / 4\pi l_0 k,$$
$$W_0 = \varepsilon V \rho_0 \pi r_0^2,$$

where W_0 is the total absorbed power, R the radius of the film within a hole of the supporting metal grid ($6.4\text{x}10^{-5}$ m), r_0 the radius of the irradiated region ($2.5\text{x}10^{-7}$ m), l_0 the specimen thickness ($4.0\text{x}10^{-8}$ m), k the thermal conductivity ($5.1\text{x}10^{-1}$ $\text{Wm}^{-1}\text{K}^{-1}$ for amorphous Ge [27]), ε the fraction of energy absorbed (usually 0.01), V the acceleration voltage, and ρ_0 the current intensity. For the present irradiation conditions, the maximum temperature rise in the irradiated area was calculated to be ~6 K (~16 K) for 75 kV (125 kV) electrons to a current density of $8.8\text{x}10^2$ A/m^2 ($13.5\text{x}10^2$ A/m^2). Our present study demonstrated that the low-temperature synthesis of Ge with a Sn concentration of ~30 at.% can be realized by electron-beam irradiation.

In conclusion, the structural changes of amorphous GeSn under electron-beam irradiation were examined by *in situ* TEM. Recrystallization was successfully induced at room temperature, and the resultant crystalline GeSn showed a diamond structure and Sn segregation was highly suppressed. From the lattice parameter, the maximum substitutional Sn concentration in the present study was estimated to be 29.7 at.%. The critical flux for amorphous-to-crystalline phase transformation became small with decreasing acceleration voltage, suggesting that the present crystallization was induced by the electron excitation effect rather than by the knock-on one. The temperature rise during irradiation was negligible; thus, it can be concluded that electron-beam irradiation is useful for realizing the low-temperature synthesis of high-Sn-concentration GeSn. Note that the grain size obtained here is <10 nm as shown in Fig. 2(b); therefore, there is a possibility that the potential of GeSn as a thin film transistor or solar cell cannot be derived. On the other hand, coarse grains (>100 nm) are formed in Fig. 2(d), although Sn segregation occurs. By optimizing the irradiation conditions, we consider that it is possible to form large GeSn grains without Sn segregation. A more extensive study is currently under way.

Acknowledgments

TEM observations using Hitachi H-7000 were supported by the Osaka University Microstructural Characterization Platform as the program “Nanotechnology Platform” of the Ministry of Education, Culture, Sports, Science and Technology (MEXT), Japan.

References

[1] S. Zaima, O. Nakatsuka, N. Taoka, M. Kurosawa, W. Takeuchi, and M. Sakashita, Sci. Technol. Adv. Mater. **16**, 043502 (2015).

[2] M. Hansen and K. Anderko, *Constitution of Binary Alloys* (McGraw-Hill, New York, 1958).

[3] R. R. Lieten, S. Decoster, M. Menghini, J. W. Seo, A. Vantomme, and J.-P. Locquet, ECS Trans. **50**, 915 (2013).

[4] R. R. Lieten, J. W. Seo, S. Decoster, A. Vantomme, S. Peters, K. C. Bustillo, E. E. Haller, M. Menghini, and J.-P. Locquet, Appl. Phys. Lett. **102**, 052106 (2013).

[5] K. Toko, N. Oya, N. Saitoh, N. Yoshizawa, and T. Suemasu, Appl. Phys. Lett. **106**, 082109 (2015).

[6] W. Takeuchi, N. Taoka, M. Kurosawa, M. Sakashita, O. Nakatsuka, and S. Zaima, Appl. Phys. Lett. **107**, 022103 (2015).

[7] R. Matsumura, H. Chikita, Y. Kai, T. Sadoh, H. Ikenoue, and M. Miyao, Appl. Phys. Lett. **107**, 262106 (2015).

[8] M. Kim, W. Fan, J.-H. Seo, N. Cho, S.-C. Liu, D. Geng, Y. Liu, S. Gong, X. Wang, W. Zhou, and Z Ma, Appl. Phys. Express **8**, 061301 (2015).

[9] W. Knaepen, S. Gaudet, C. Detavernier, R. L. Van Meirhaeghe, J. J. Sweet, and C. Lavoie, J. Appl. Phys. **105**, 083532 (2009).

[10] N. Uchida, T. Maeda, R. R. Lieten, S. Okajima, Y. Ohishi, R. Takase, M. Ishimaru, and J.-P. Locquet, Appl. Phys. Lett. **107**, 232105 (2015).

[11] R. Takase, M. Ishimaru, N. Uchida, T. Maeda, K. Sato, R. R. Lieten, and J.-P. Locquet, J. Appl. Phys. **120**, 245304 (2016).

[12] V. Heera, R. Kögler, W. Skorupa, and J. Stoemenos, Appl. Phys. Lett. **67**, 1999 (1995).

[13] R. Nakamura, M. Ishimaru, H. Yasuda, and H. Nakajima, J. Appl. Phys. **113**, 064312 (2013).

[14] R. Nakamura, T. Shudo, A. Hirata, M. Ishimaru, and H. Nakajima, Scr. Mater. **64**, 197 (2011).

[15] R. Nakamura, M. Ishimaru, A. Hirata, K. Sato, M. Tane, H. Kimizuka, T. Shudo, T. J. Konno, and H. Nakajima, J. Appl. Phys. **110**, 064324 (2011).

[16] J. Kanasaki, E. Inami, K. Tanimura, H. Ohnishi, and K. Nasu, Phys. Rev. Lett. **102**, 087402 (2009).

[17] M. Ishimaru, I.V. Afanasyev-Charkin, and K.E. Sickafus, Appl. Phys. Lett. **76**, 2556 (2000).

[18] M. Ishimaru, Y. Hirotsu, M. Tang, J. A. Valdez, and K. E. Sickafus, J. Appl. Phys. **102**, 063532 (2007).

[19] M. Okugawa, R. Nakamura, M. Ishimaru, K. Watanabe, H. Yasuda, and H. Numakura, J. Appl. Phys. **119**, 214309 (2016).

[20] M. Okugawa, R. Nakamura, M. Ishimaru, H. Yasuda, and H. Numakura, J. Appl. Phys. **120**, 134308 (2016).

[21] Z. H. Cao, P. Liu, X. K. Meng, S. C. Tang, and H. M. Lu, Appl. Phys. A **94**, 393 (2009).

[22] T. Kimura, M. Ishimaru, M. Okugawa, R. Nakamura, and H. Yasuda, Microsc. Microanal. 23 (Supplement 1), 2047 (2017).

[23] I. Jencic, I. M. Robertson, and J. Skvarc, Nucl. Instrum. Methods Phys. Res., Sect. B **148**, 345 (1999).

[24] M. Liu, L. Xu, and X. Lin, Scanning **16**, 1 (1994).

[25] X.-w. Du, M. Takeguchi, M. Tanaka, and K. Furuya, Appl. Phys. Lett. **82**, 1108 (2003).

[26] C. L. Chen, K. Arakawa, and H. Mori, Scr. Mater. **63**, 1013 (2010).

[27] D. G. Cahill and R. O. Pohl, Phys. Rev. B **37**, 15 (1988).

Figure captions

Fig. 1. (Color online) (a) High-resolution TEM image and SAED pattern of as-sputtered amorphous GeSn. (b) EDX spectrum obtained from the same specimen. The Mo signal originates from the grid. (c) Relationship between Sn concentration and the number of Sn chips.

Fig. 2. SAED patterns and bright-field TEM images of the GeSn thin films crystallized by a 75 keV electron beam with fluxes of (a, b) 8.7×10^{21} and (c, d) 7.9×10^{22} e/(m^2/s). The Sn concentration is 22.8 at.% in the as-sputtered amorphous state.

Fig. 3. (Color online) Threshold flux required for amorphous-to-crystalline phase transformation as a function of Sn concentration in amorphous state. Circles and squares denote the results of 75 and 125 kV electron irradiations, respectively.

Fig. 4. (Color online) SAED patterns of GeSn crystallized by electron-beam irradiation with a threshold flux required for amorphous-to-crystalline phase transformation in Fig. 3. The Sn concentrations are (a) 8.2, (b) 20.0, (c) 22.8, and (d) 40.2 at.% in the as-sputtered amorphous GeSn. To observe a weak halo ring easily, the contrast is reversed. (e) Sn concentration of crystallized GeSn estimated from the lattice parameter (open circles). For comparison, the Sn concentration of as-sputtered specimens estimated by EDX spectroscopy is also plotted as closed circles.

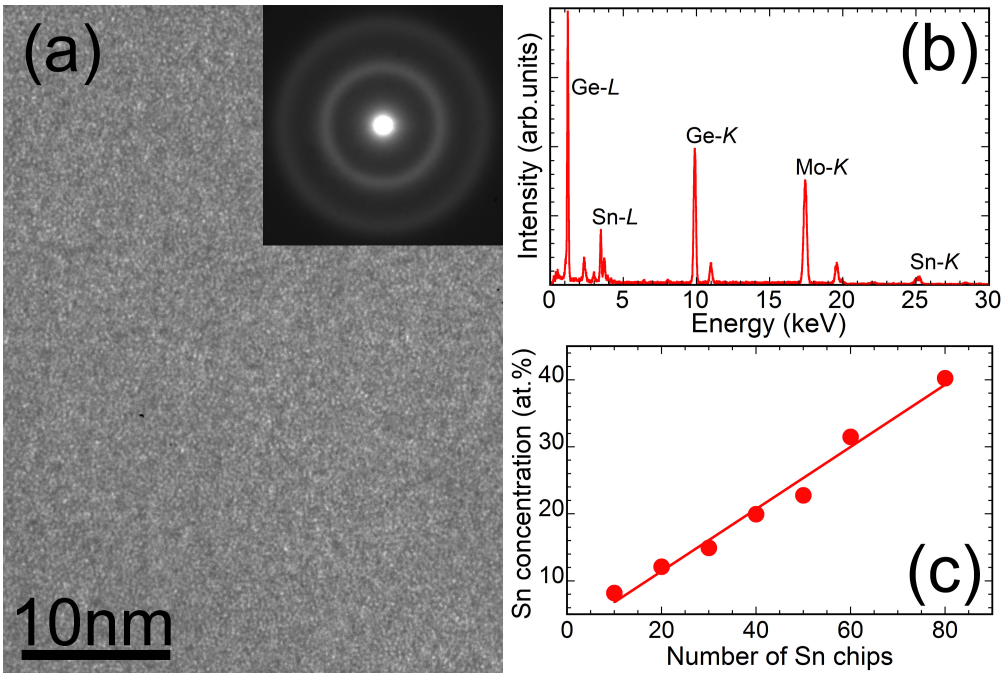
(a)
10nm
(b)
Intensity (arb.units)
Ge-L
Sn-L
Ge-K
Mo-K
Sn-K
0
5
10
15
20
25
30
Energy (keV)
(c)
Sn concentration (at.%)
10
20
30
40
0
20
40
60
80
Number of Sn chips

Fig. 1

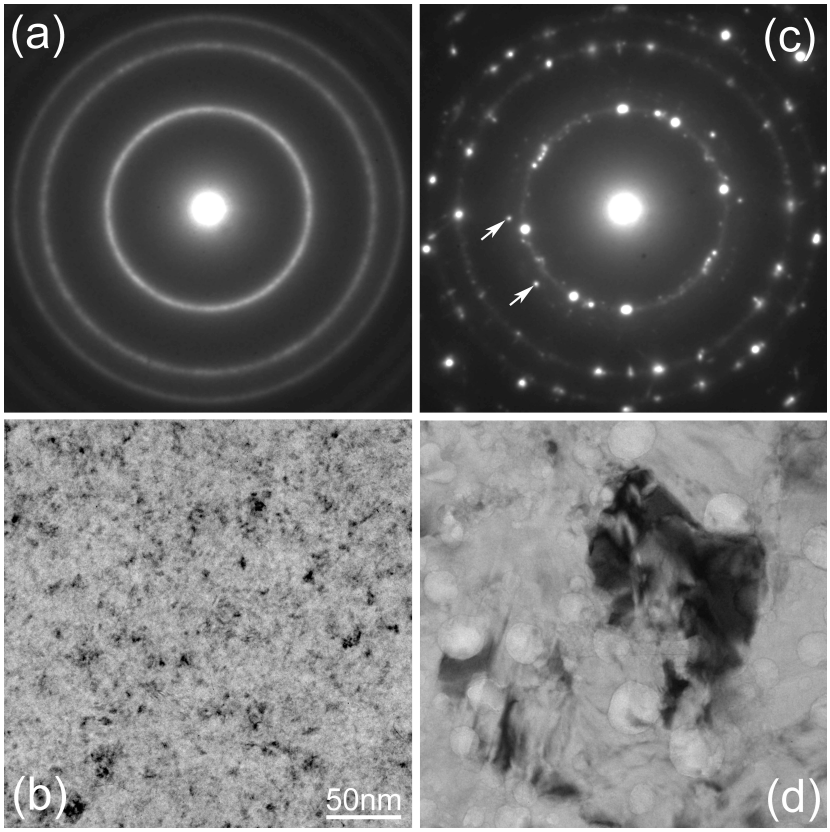

Fig. 2

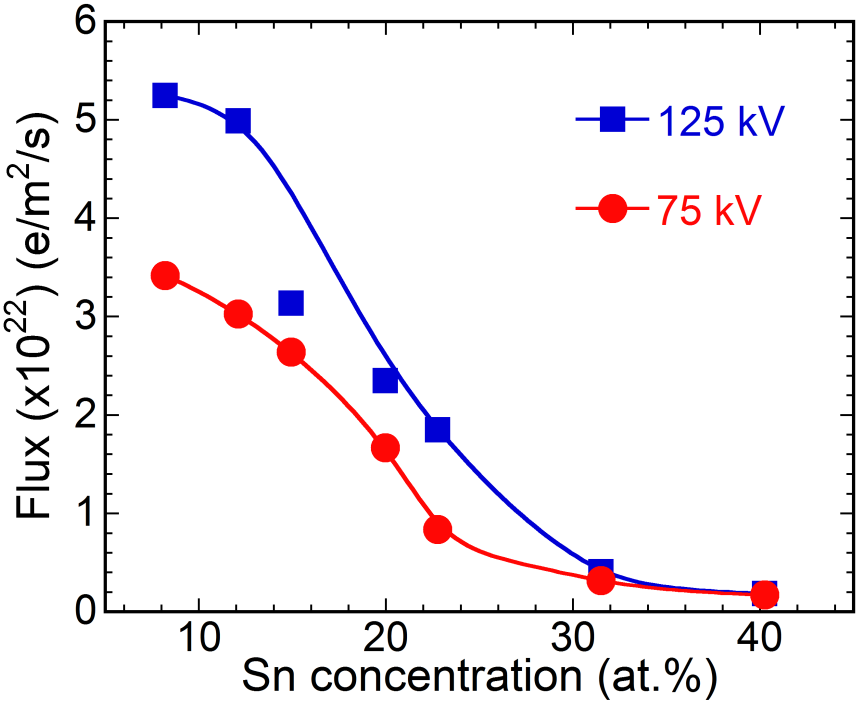
Flux (x10^22) (e/m^2/s)
Sn concentration (at.%)
125 kV
75 kV
0
1
2
3
4
5
6
10
20
30
40

Fig. 3

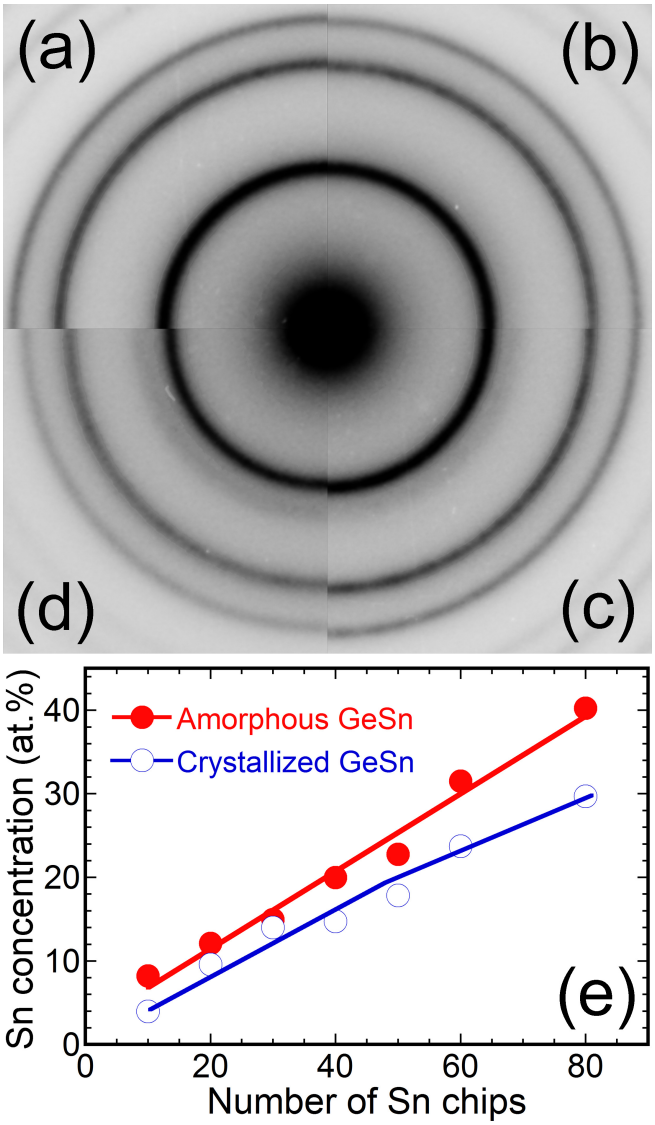
(a)
(b)
(d)
(c)
Amorphous GeSn
Crystallized GeSn
Sn concentration (at.%)
Number of Sn chips
0
10
20
30
40
0
20
40
60
80
(e)

Fig. 4